Wavelength shifts in Erbium doped glass microspherical Whispering Gallery Mode lasers

Carole Arnaud, Mohamed Boustimi [a] and Patrice Féron[1]

Laboratoire d'Optronique, CNRS - UMR 6082 "FOTON", ENSSAT, 6 rue de Kerampont 22300 Lannion, France

April 2004

Abstract. We have succeeded in continuous-wave laser oscillation on $^4I_{13/2} \rightarrow {}^4I_{15/2}$ transition of Er^{3+} ions around 1550 nm in microspheres fabricated with Erbium doped fluoride "ZBLALiP" and phosphate "Schott" glasses. The microsphere lasers have been studied under pumping at 1480 nm. Whispering Gallery Mode laser spectra were analyzed for different sphere diameters. Wavelength Red-shift effect of both fluorescence and laser spectra was experimentally observed in Er^{3+} doped phosphate glass when the pump power was increased, originating from thermal effects. We showed coupling effect between microspherical laser and an external cavity made by a metallic mirror. We observed line shift to lower wavelengths due to optical feedback effect. A general overview of the current state of the art in microspheres is given as well as a more general introduction.

PACS. 42.55.Sa Microcavity lasers – 42.60.Fc Laser tuning – 42.70.Hj Laser materials

1 Introduction

Microspherical resonators have attracted considerable interests for investigation of fundamental processes ranging from cavity quantum electrodynamics (QED) [1,2] to nonlinear optics [3], and in more applied areas such as photonics [4] and chemical/biological sensing [5,6]. Light can be confined efficiently in the high quality factor ($Q=\nu/\Delta\nu$) small volume whispering-gallery-modes (WGMs) observed in spherical dielectric microresonators if the refractive index of the material of the sphere is larger than the one surrounding it. Successive total internal reflections off the concave inner surface confine the light into a thin ring close to the equator. These high-Q ring modes have been observed and studied extensively in droplets [7]. It was soon recognized that the field enhancement caused by the strong confinement of the light in this modes combined with their high quality factors could lead to strong cavity-QED effects. Stimulated Raman scattering, to name but one, has been observed in small CS2 droplets with a threshold of just three photons per mode [8]. Whispering Gallery Modes have also been used to produce lasers in microdisks [9] and to enhance the spontaneous emission of quantum dots in micropillar structures [10]. However, semiconductor microdisks and pillars can only operate in the low-Q regime and microdroplets suffer unfortunately from evaporation and gravitational pull.

Send offprint requests to: feron@enssat.fr

[a] *Present address:* Cork Institute of Technology, Rossa Avenue,

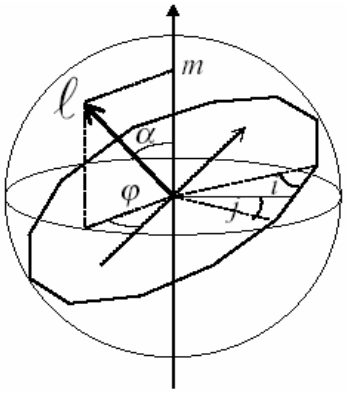

Fig. 1. Ray of light propagation by TIR. Definition of complementary angles *i* and *j*.

Since the pioneering works of Garret *et al* [11] on Sm^{2+}: CaF_2 spheres and the first laser oscillation in a solid state sphere demonstrated by T. Baer [12] with large Nd:YAG spheres (5 *mm* in diameter), rare earth doped glass lasers became subject to numerous studies and significant progress has been achieved in the past decade and have been demonstrated as potentially compact laser source [13-15]. After a brief introduction to the physics of the whispering-gallery modes, we will describe recent experiments on the lasing properties of Erbium doped microspheres at room temperature. Lasing action around 1550 nm was observed in these spheres by using a 1480 nm pump source and a tapered- fiber to couple in the pump and out the emitted signal. Red-shift effect on the wavelengths of both fluorescence and laser spectra is experimentally observed when the pump power is increased, originating from thermal effects. A spectroscopic technique based on the green upconversion fluorescence [16] is used to compute a loading effective temperature for a new kind of Erbium doped heavy fluoride glass Er:ZBLALiP microsphere. This method allows us to calibrate the glass properties in terms of the thermal expansion as well as the variation of the refractive index. We report the preliminary results of our investigation on the interaction between the WGMs of glass spheres and an external metallic mirror. WGMs laser spectra were analyzed for different glasses, several spheres diameters and for two metallic mirrors and we showed coupling effect between microspherical laser and the external cavity made by the mirror. To be more precise, we observed a line shift to lower wavelengths due to optical feedback effect. These results are not in full agreement with the published results [17,18] on the WGMs of a sphere resting on or close to a metallic surface.

2 Whispering gallery modes in microspheres

This section gives a short overview of the general properties of whispering gallery modes (WGMs). A more detailed account of the theory of the WGMs and on experiments performed on microspheres can be found in [3,7].

A transparent dielectric sphere can sustain WGMs if its circumference is larger than a few wavelengths. In the optical domain, whispering-gallery modes can be viewed as high angular momentum electromagnetic modes in which light propagates by repeated total internal reffection (TIR) surface at grazing incidence with the proper phase condition after circling along the sphere surface. The trapped ray propagates close to the surface, and traverses a distance $\approx 2\pi a$ in a round trip. If one round trip exactly equals ℓ wavelengths in the medium (ℓ = integer), then one expects a standing wave to occur. This condition translates into $2\pi a \approx \ell(\lambda / N)$ since λ / N is the wavelength in the medium. In terms of size parameter the resonance condition is $x = 2\pi a/\lambda \approx \ell / N$. The number of wavelengths ℓ in the circumference can be identified as the angular momentum in the usual sense. Indeed, let us consider the ray in figure 1 as a photon. Its momentum is $p = \hbar k = \hbar 2\pi N/\lambda$ where *k* is the wave number. If this ray strikes the surface at near-glancing incidence $i \approx \pi/2$, then the angular momentum, denoted as $\hbar\ell$, is $\hbar\ell \approx ap = a2\pi\hbar N/\lambda$.

For lower incidences, one expects other resonances at frequencies very close and characterized by the

radius of the caustic $r_1 = a\cos j$ under condition $(a/N < r_1 < a)$.

The modes can readily be derived from Maxwell's equations solved in spherical coordinates. Following the Hansen's method [19], solutions of the vectorial Helmholtz equation lead to fields for both polarizations:

$$E_{\ell m}^{TE}(r) = E_0 \frac{f_\ell(r)}{k_0 r} \mathrm{X}_\ell^{\mathrm{m}}(\phi,\varphi) \quad (1)$$

$$B_{\ell m}^{TE}(r) = \frac{iE_0}{-c}\left[\frac{f_\ell(r)}{k_0^2 r}\mathrm{Y}_\ell^{\mathrm{m}}(\phi,\varphi) + \sqrt{\ell(\ell+1)}\frac{f_\ell(r)}{k_0^2 r^2}Z_\ell^{\mathrm{m}}(\phi,\varphi)\right] \quad (2)$$

$$E_{\ell m}^{TE}(r) = \frac{E_0}{N^2}\left[\frac{f_\ell(r)}{k_0^2 r}\mathrm{Y}_\ell^{\mathrm{m}}(\phi,\varphi) + \sqrt{\ell(\ell+1)}\frac{f_\ell(r)}{k_0^2 r^2}Z_\ell^{\mathrm{m}}(\phi,\varphi)\right] \quad (3)$$

$$B_{\ell m}^{TE}(r) = -\frac{iE_0}{c}\frac{f_\ell(r)}{k_0 r}\mathrm{X}_\ell^{\mathrm{m}}(\phi,\varphi) \quad (4)$$

With $f_\ell(r) = \psi_\ell(Nk_o r)$ for r<a and $f_\ell(r) = \alpha\psi_\ell(k_o r) + \beta\chi_\ell(k_o r)$ for r>a. $\psi_\ell(\rho) = \rho j_\ell(\rho)$ and $\chi_\ell(\rho) = \rho n_\ell(\rho)$ where j_ℓ and n_ℓ are respectively spherical Bessel and Neumann functions. X_ℓ^m, Y_ℓ^m, Z_ℓ^m are vectorial spherical harmonics. Continuity of tangential components of the fields

allows to find equations for the positions of resonances. By going through the standard Mie scattering formalism [20], the resonance condition can be written as :

$$P\frac{J'_{\ell+1/2}(Nx)}{J_{\ell+1/2}(Nx)} = \frac{N'_{\ell+1/2}(x)}{N_{\ell+1/2}(x)}$$

where $P = N$ for TE polarization ($P = N^{-1}$ for TM) and $\ell + 1/2$ comes about in translating the spherical Bessel and Neumann functions to their cylindrical counterparts. The quantities in Eq.5 can be expressed as asymptotic series[21] in powers of $(\ell + ½)^{-1/3}$. This leads to the first terms of the resonances expressed in size parameter:

$$Nx_{n,\ell} = \ell + ½ - \left(\frac{\ell+1/2}{2}\right)^{1/3}\alpha_n - \frac{P}{\sqrt{N^2-1}} + \ldots \quad (6)$$

where α_n are zeros of Airy function $Ai(-z)$.In short, once the polarization of the mode ssigned,WGMs are described by three integers *n;* ℓ and *m*. The two quantum numbers ℓ and *m* (with $m = -\ell, \ldots + \ell$) describe the total angular momentum and its projection upon the reference axes respectively. Quantum numbers *m* of opposite sign correspond to waves propagating in opposite directions along the perimeter of the sphere. The modes offering the highest polar confinement and thus the smallest mode-volume correspond to values *[m]* close to ℓ. The radial confinement of the WGMs is characterized by the quantum number *n*, the number of antinodes of the field amplitude. A more detailed account of the effective potential approach leading to this radial number has been analyzed by Nussenzveig[22].

Equation 6 allows to precise the main characteristics of WGM spectrum. First, the spectrum is quasi-periodic *versus* ℓ, this corresponds to a pseudo-Free Spectral Range (FSR) $\Delta_o = c/2\pi Na$. Second, the spacing between modes having same quantum numbers but different polarizations is $\Delta\nu_{n,\ell}^{TE-TM} = \Delta_o\sqrt{N^2-1}/N$. The greatest change of frequency is produced by variation of *n* (as example with $\ell \approx 250$ the mode separation $\sim 10\Delta_o$) it decreases when *n* values grow up. Small ellipticities lead to a quasi-equidistant mode family characterized by $\Delta\nu/\Delta|m|$.

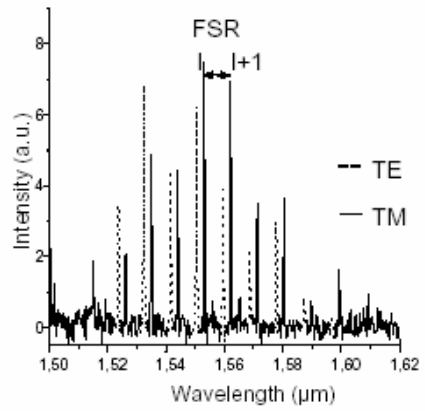

Fig. 2. Fluorescence WGM spectrum (n = 1) of Er:ZBLAN sphere excited by prism

The mode with the longest lifetime and the smallest volume is ($\ell = \ell_{\max}$; $|m| = \pm \ell$; $n = 1$). It is confined near the bottom of the potential well, *i.e.* as close as possible to the surface of the sphere. Light trapped in these modes can escape out of the sphere only by tunnelling across the potential barrier due to the combination of the index discontinuity with the centrifugal barrier. The very short evanescent tail of the quasi-bound state ($n \cong 1$) implies a very weak coupling to the outside medium and thus extremely high quality factors Q.

2.1 Coupling light into whispering gallery modes

The very high diffraction-limited Q of the fundamental modes of large sphere ($a \geq 20\mu m$) implies that free space coupling to the microspheres is very inefficient. Efficient coupling to WGMs not only requires to adjust the frequency of the excitation beam to a WGM resonance. The excitation beam should also have an angular momentum (with respect to the center of the sphere) which matches the angular momentum of this mode. This last condition is not met with a free propagating beam even it is focused near the edge of the sphere [23]. The potential barrier created by the index discontinuity at the surface of the sphere confines almost all the field to the inside of the sphere.

However, a short evanescent tail of the electromagnetic field protrudes from the sphere. If a aterial of high refractive index is brought into this evanescent wave some of the light will tunnel across the gap between the material and the sphere. If we are interested to the most confined modes with low radial numbers, only frustrated total internal reection provides an efficient excitation scheme.

This can be achieved with a prism of high refractive index (N_p) almost in contact with the sphere. If the incident beam hits the prism surface with an angle θ close to the crical angle $\theta_c = \arcsin(N/N_p)$ so that its angular momentum is $N_p ka \sin\theta \approx Nka$ its light can be fed into a WGM.

This method has been used in the pioneering work of Braginsky *et al* [24] for passive microspheres and by Sandoghdar *et al* [14] and us [15] in a slightly different geometry for active microspheres. Figure 2 presents fluorescence spectrum around 1.55 μm obtained with a microsphere 56 μm in diameter doped with 0.2 % by weight of Erbium under such coupling by prism. This spectrum presents a discrete feature which is characteristic of the collection through WGMs, with mainly two series of peaks associated to TE and TM modes. The measured pseudo Free spectral range (Δ_0) and spacing between modes having same quantum numbers but different polarizations $\Delta\nu_{n,l}^{TE-TM}$ are close to the calculated values given by equation 6.

3 Experiments on microspheres in Lannion

3.1 Experimental set-up

For both passive and active microspheres other different coupling techniques, such as tapered fibers [25-27],half block couplers [28], angle polished fiber couplers [29] and waveguides [4] have been experimentally demonstrated. Our experiments are focused on the optical transition ${}^4I_{13/2} \rightarrow {}^4I_{15/2}$ at 1.55 μm of Erbium doped spheres. Among the different pumping wavelengths which can be used (810nm, 975nm and 1.48μm) [30], we chose 1.48μm in order to obtain a good overlap between the pump and laser mode volumes. The experiments described here are all based on the half-taper coupler method [27]: the light is coupled into and out of the sphere *via* an half-taper for direct fiber coupling. Coupling of fluoride or phosphate microspherical lasers differs on two main points from coupling of passive silica spheres: (i) the refractive index of the sphere materials are different (example : $N_s \cong 1.5$ ($\cong 1.45$) for ZBLA (silica) at wavelength $\lambda = 1.55\mu m$) (ii) the optimum coupling with two wavelengths, $\lambda = 1.48\mu m$ for the pump and $\lambda = 1.55\mu m$ for the laser signal is not the same. Using the method described by Knight [25] we calculated how to match the propagation constant of the appropriate mode in the

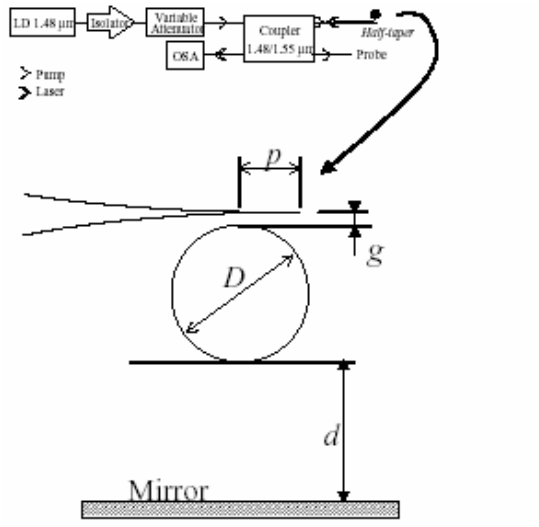

Fig. 3. Experimental set-up and geometry of the coupling between a sphere and a mirror

tapered fiber to the propagation constant of the WG modes at the surface of the sphere for both wavelengths. These calculations were made for a fiber drawn gradually to form a narrow thread but they also can be used for a fiber tapered till the break (half-taper). Calculations show that: (i) a good coupling is obtained for those spheres characterized by specific (N_s; a) for wavelengths λ (ii) in our case, as the pump wavelength is close to that of the laser field, a single taper or half-taper allows to couple both fields in and out the microspherical laser. The fiber coupling experiments were performed with half-tapered fiber, that we obtained by heating and stretching standard telecommunication fiber (single mode at 1.55 μm) until breaking, using a fusion optical splicing system. The drawn length was typically 850 μm, and the taper end reduced to 1.5 μm in diameter. The experimental setup (see Fig.3) was realized with standard fiber-optic components spliced or connected with APC connectors. Mounting spheres on microtranslations brought the equator region in contact with the evanescent field surrounding the taper. The pump device was based on a fiber pigtailed multimode laser diode (maximum output power, 1 *W*) operating around 1.48 μm, an isolator that prevent feedback into the laser diode, and an X-coupler at 1.48-1.55 μm. The X-coupler allowed us to use the same fiber to pump and to collect the fluorescence or the laser signal. The X-coupler enabled us to have a pump reference that was separated from the laser signal (noted as *probe*), which was analyzed with a 70 *pm* resolution optical spectrum analyzer (OSA). For the experiment with an external cavity, the metallic at mirror was mounted on microtranslations below the micro-sphere (Fig.3). The same experimental setup was used for experiments on both ZBLALiP and Phosphate glasses.

3.2 Cross-sections and gain properties

Er:ZBLALiP glass, their spectroscopic properties and experiments on different glass samples with doping rate in Erbium varying from 0.01 *mol.*% to 6 *mol.*% have been described in a previous paper [31]. The phosphate glass used, was an Er^{3+}/Yb^{3+} co-

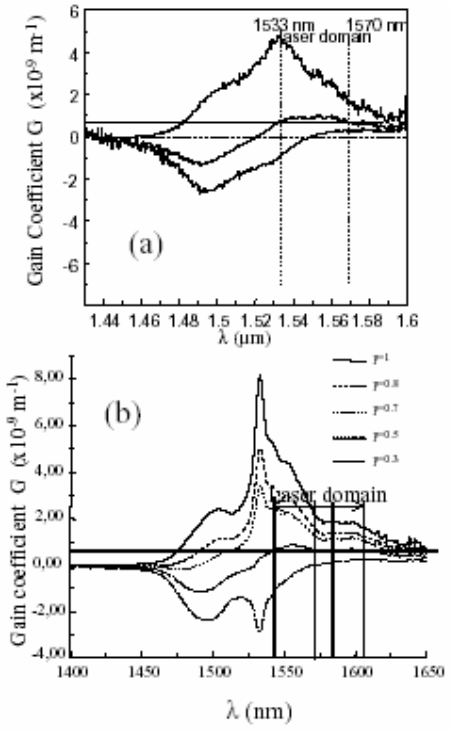

Fig. 4. Gain Spectra (a) for ZBLALiP glass Erbium doped with concentration of 0:05%*mol* - (b) for Er3+/Yb3+ co-doped phosphate glass

doped phosphate glass (Schott IOG- 2) doped with 2% weight of Er_2O_3 and co-doped with 3% weight Yb_2O_3. Absorption spectra were recorded on a double-beam Cary 17 spectrometer with a resolution better than 0.1 *nm* for the fluoride glass.We used a Cary 9000 spectrometer for the phosphate glass. The emission cross section spectra were derived using the reciprocity relation of McCumber's theory [32] where absorption and emission cross sections are related by

$$\sigma_a(\lambda) = \sigma_e(\lambda) \cdot \frac{Z_L}{Z_U} \exp\left[\frac{hc}{k_B T}\left(\frac{1}{\lambda} - \frac{1}{\lambda_0}\right)\right] \qquad (7)$$

where Z_L, Z_U are the partition functions of the upper and lower levels, λ_0 the wavelength corresponding to the two lowest Stark levels of the $^4I_{13/2}$ and $^4I_{15/2}$ levels. h is the Planck's constant, c the light velocity, k_B the Boltzmann's constant and T the temperature in Kelvin. Computation of Z_L, Z_U needs the spectroscopic values of both levels of Erbium ion, *i.e.* their degenerencies and Stark-level energies (see Eq.2 in Ref. [32]). In general, such Stark components of Er^{3+} doped glasses can be deduced from the low temperature absorption-emission spectra [33]. Based on these absolute cross section spectra, the net gain spectra $G(\lambda, p)$ can be computed in terms of the pumping level [34] as the following:

$$G(\lambda, p) = n_{Er} \cdot \left[p\sigma_e(\lambda) - (1-p)\sigma_a(\lambda)\right] \qquad (8)$$

where p is the fractional factor of the excited Erbium ions in the metastable level $^4I_{13/2}$. It is important to note that p is an excitation parameter averaged over temperature due to Stark effects of both the upper and lower levels. $G(\lambda, p)$ represents the gain spectra at room temperature which is applicable to the lasing threshold condition where there is no significantly increase of temperature. Figures 4 present the gain spectra calculated for several values of p for Er:ZBLALiP glass 0.05 *mol*% doped in Erbium and for Er/Yb phosphate glass. We note (Fig.4 - a) a laser domain extending approximately from 1533 to 1570 *nm* for ZBLALiP glass and from 1542 to

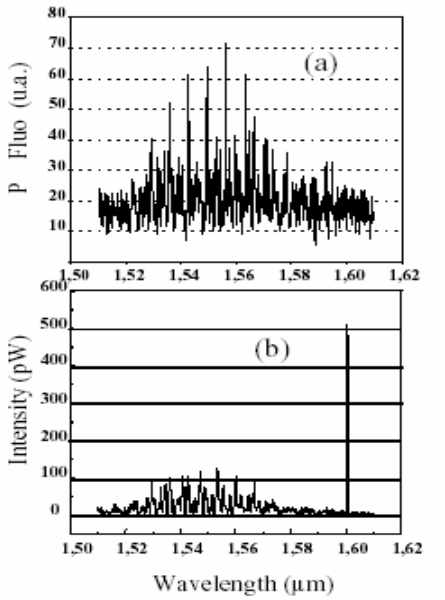

Fig. 5. Er/Yb phosphate glass sphere (a) Fluorescence WGM spectrum - (b)laser effect @ 1601 *mn* at threshold

1605 *nm* for the Schott IOG-2 glass (Fig.4 - b). Spheres were produced by fusion of glass powders with a microwave plasma torch. Powders are injected axially and melt when passing through the flame, superficial tension forces giving them their spherical form. Free spheres with a diameter which varies from 10 to 200μm are collected a few centimeters below. Then, they are glued at a stretched tip of optical fibers (~ 20μm in diameter) which allows to manipulate them easily and to insert them in the optical setup.

3.3 Results on free spheres

Figures 5 show different features of WGMs spectra, below and above the laser threshold for Er^{3+}/Yb^{3+} co-doped phosphate glass micro-sphere with a diameter $D \sim 70\mu m$. As demonstrated in a previous paper [27], for any sphere diameter and materials (fluoride or phosphate glasses), the optical spectrum of the micro-sphere below the threshold shows an enhancement of the fluorescence intensity and a higher peak density than those obtained with a prism. The taper is characterized by a conic

geometry and a varying effective index, thus the evanescent field structure is more complicated than the evanescent field obtained with a prism and more modes can thus be excited in the sphere which qualitatively justify the large number of lines on the fluorescence spectrum (Fig.5 - a). Nevertheless, for sufficiently large sphere diameter in respect to the wavelength (typically diameter $D > 20\ \lambda$) we can use an analysis similar to that used for excitation by a prism [15] on the basis of asymptotic expression (Eq.6) for WGM size parameters. This standard analysis shows that these series of peaks can be assigned to several families of modes instead of one predominant family when a prism is used, each of them having the same radial order *n* but different polarizations and angular momenta ℓ. When increasing the pump intensity we obtained laser oscillation (Fig.5 - b).

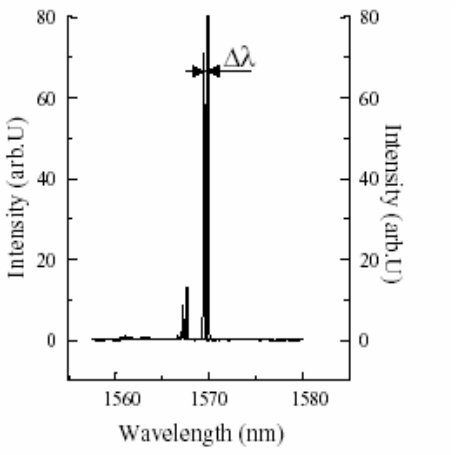

Fig. 6. Red-shift of laser lines in Er/Yb phosphate glass sphere

As demonstrated in previous work on excitation by prism [15] a fixed gap value between the excitation device and the sphere enables to select the emission domain. We obtain this by varying the gap *g* and the position *p* between the tip of the half taper and the sphere in the coupling scheme (Fig.3). For a large gap value and a low pumping ratio we have obtained a laser emission around 1601 *nm* (Fig.5 - b). For a lower gap value associated to an higher pumping ratio we have obtained single mode or multimode laser effects for lower wavelengths.

4 Wavelength shift

4.1 Effect due to temperature

Red shift effect on the wavelength of WGMs is experimentally observed when the pump power is increased. This effect was previously observed and explained by a simple model in Er/Yb phosphate microchip laser [16] and Er:ZBLALiP microspherical laser [35]. We can note that thermal tuning of WG modes was proposed and measured for the first time (0.1% tuning of the eigenfrequency) by Vyatchanin *et.al* [36]. The laser spectra were analyzed by an Optical Spectrum Analyzer with a resolution of 70 *pm* as the pump

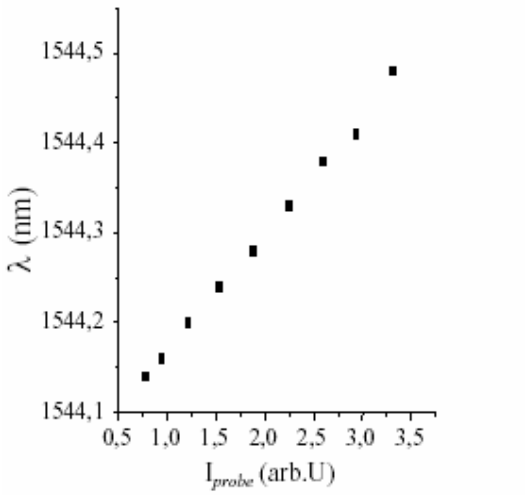

Fig. 7. Red-shift of a fluorescence WGM line in Er/Yb phosphate glass sphere

power was increased under 1480 *nm* pumping.

The two wavelengths at 1567.1 *nm* and 1569.4 *nm* when the *probe* intensity is 0.5, shift further to 1567.6 *nm* and 1569.9 *nm*, respectively, under 3.5 excitation (Fig.6). Similar red-shift behaviours have also been observed for other lasing or non-lasing WGMs (Fig.7) as the pump intensities increased and this for every sphere diameter. It should be noted that all WGMs shift by almost 0.5 *nm* towards

longer wavelength under the *probe* power domain extending from 0.5 to 3.5. In our simple model [16] the microspherical laser consists of an active cavity within which phonons associated with the non radiative decay between the manifolds of Erbium ions,*e.g.*,$^4I_{11/2} \rightarrow ^4 I_{13/2}$, and between the intra-Stark levels of the laser manifolds,*i.e.*,$^4I_{15/2}$ and $^4I_{13/2}$, create thermal deposition and thus heat the microsphere. An increase of cavity temperature ΔT results not only in an expansion Δd of the micro-sphere cavity length but also in a change of index of refraction ΔN. Both changes then affect the lasing condition and the wavelength shift $\Delta\lambda$ of every WGM as the cavity temperature rises by ΔT can be written as [16].

Here N and d are constant values which are referenced to the room temperature, or if one wants to be more precise, to the temperature corresponding to the threshold for oscillation. $\partial N/\partial T$, $\partial d/\partial T$ are change ratio with respect to temperature for the index of refraction and thermal expansion of the Er/Yb co-doped phosphate glass. The calibration of the cavity temperature by use of the upconversion intensity ratio of two lines originating from Erbium levels $^4S_{3/2}$ and $^2H_{11/2}$ will be subject for further investigation.

4.2 Effect due to coupling with an external cavity

The studies on coupling between microresonators concern essentially coupled ring resonators. Such resonators are more amenable to integrated optical fabrication approaches. Serial and parallel sequences of coupled high-Q microring resonators have been studied and almost modelled using a transfer matrix approach [37,38] but concerning the microsphere, most of the works were performed in studying light scattering by small particles where WGMs correspond to so called Morphology Dependent resonances (MDRs) and in a recent work Smith *et al.*[39] demonstrated that the MDRs split into N higher-Q modes for a structure consisting of N-layered microsphere or N-coupled ring resonators. They demonstrated numerically this splitting using

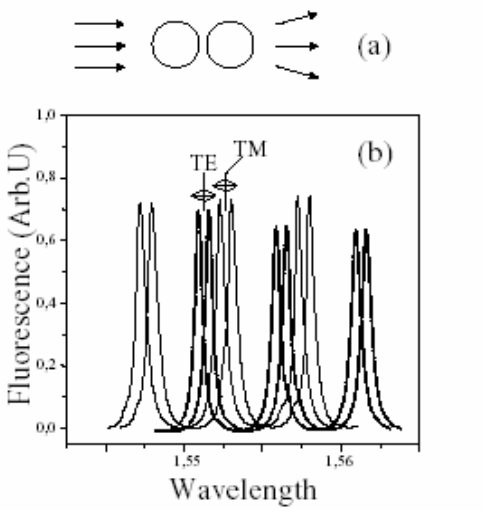

Fig. 8. (a) Geometry of Fuller's problem (b) splitting of WGMs expected in fluorescence spectrum

an iterative approach to Mie scattering theory of a bisphere system developed by Fuller [40,41]. The physical system considered in this analysis and expected results on fluorescence spectrum are illustrated in Fig.8. Based also on Mie theory of scattering [42] and numerically evaluated Johnson's theoretical treatment[18] of the MDR's of a dielectric sphere on or near a plane of infinite conductivity examines how the locations and widths of the resonances change as the sphere approaches the surface. If the sphere is initially located at a distance d that is more than approximately $2D/3$ away from the point of contact with the conducting plane, the resonances will have the same locations and widths as they do in an isolated sphere. Then, as the sphere is brought closer to and eventually in contact with the surface, the locations and widths of the resonances change. The locations of the TE-mode resonances shift to higher size parameters (*i.e* Blue-shift in wavelength), the TM-mode resonances shift to lower lower size parameters (*i.e* Red-shift in wavelength) and the widths of both types of resonance increase. The physical system considered in this analysis and expected results on fluorescence spectrum are illustrated in Fig.9. Most of the change in location and width occurs when the sphere is quite

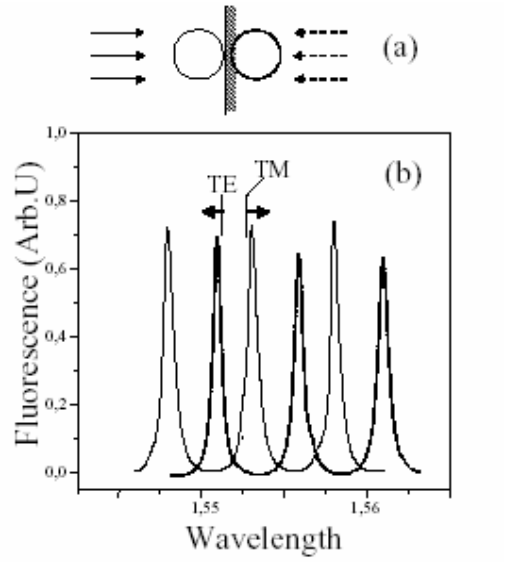

Fig. 9. (a) Geometry of Johnson's problem (b) shifts ofWGMs expected in fluorescence spectrum

close to the conducting plane. Approximately 90% of the total resonance shift occurs when the distance from the point of contact is less than 0.05 of the diameter of the sphere.

In short, if we ignore the incident and scattered waves, the effective potential approach of Nussenzveig [22] can explain why, even the bisphere system studied by Fuller is quite similar to the system of sphere and image sphere used by Johnson, Fuller observed a resonance split, whereas Johnson observed not a split but merely a shift in the resonance location. In this approach, as mentioned in section 2, for an isolated sphere, the radial equation is very similar to the Schrödinger equation with a pocket-like pseudo potential due to the refractive index discontinuity $N - 1$ at the surface of the sphere. The mirror associated to a mirror reection symmetry operation gives an even symmetric potential (Fig.10). Thus, we obtain symmetric Ψ_g and antisymmetric Ψ_u eigenstates associated respectively to blue-shifted (symmetric) and red-shifted (antisymmetric) wavelengths. If we assume that the coupling between the sphere and its image does not affect the polarization of the WGMs *e.g* no difference between TE and TM modes except on resonance locations, such model explains the

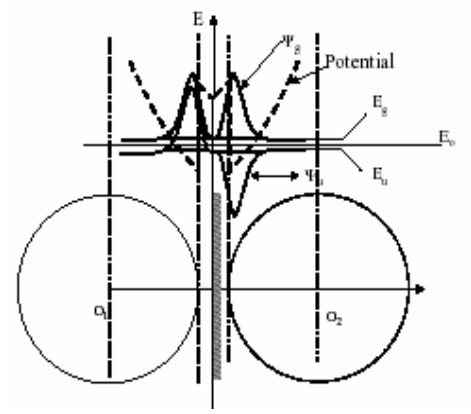

Fig. 10. Effective potential and functions associated to the problem

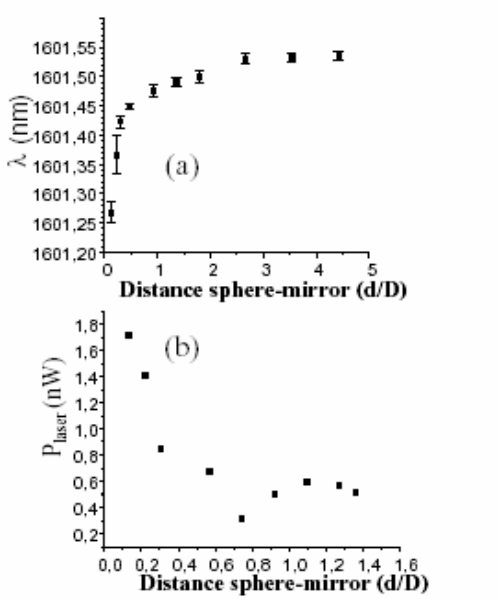

Fig. 11. (a) Blue-shift at 1601 *nm* (b) laser intensity *vs* spheremirror distance (*d=D*)

splitting on resonances for both polarization predicted by Fuller. If we take into account the infinite conductivity of the mirror which leads to a resulting electric field perpendicular to the mirror and the vector aspect of TE and TM modes *e.g* the electric field is quasi-tangential to the sphere for TE modes (quasi-radial for TM modes) for a large diameter ($D > 20\lambda$), we can see how TE modes are associated only to symmetric states and TM to

antisymmetric states. This explains the behavior on resonance locations predicted by Johnson. Such a simple model does not take into account the metallic properties of the mirror and it seems to be reasonable to consider the coupling of the TM resonances (electric field normal to the surface) to the surface waves of the silver substrate and would explain the TM mode quenching observed by Hill *et al.*[17].

4.3 Experimental results

In order to make a comparison with the experimental work of Hill *et al.* we used a silver mirror with no dielectric coating over the reective surface. This seems to be the closest approximation to the idealized case of the perfect mirror of infinite conductivity for which the method of images is strictly valid [18]. The use of a high doping rate Er^{3+}/Yb^{3+} phosphate glass (2% weight of Er_2O_3) leads to a high level of fluorescence signal and this glass seems to be a good candidate to observe the effects of the metallic mirror on the fluorescence and under a high pumping rate we obtained laser effects as seen in section 3.3.

At this point, it is important to say that with our actual experimental setup, we cannot approach the mirror closer than $d = 3.5\mu m$ and for our typical size of sphere ($D \sim 70\mu m$) $d_{min}/D = 0.05$ we cannot explore the zone where Johnson predicted 90% of the effect. However, we noticed an inuence of the mirror on both fluorescence and laser lines for distances up to 5 *D*. With a coupling such we obtained laser emission around 1600*nm* (see section 3.3) under a fixed pump power value we approached the mirror from $d = 175\mu m$ to $d = 7\mu m$ and we observed a line shift of almost 0.3*nm* towards the lower wavelength (Fig.11-a) associated to an enhancement of the intensity (Fig.11-b). Under the same experimental procedure, for a laser action at lower wavelength ($\lambda_{laser} \sim 1566$ *nm*), the mirror approach induced the same "blue shift" but also caused the laser extinction (Fig.12-a). This latter effect was confirmed by study of the threshold behavior for each sphere-mirror distance. For this wavelength we observed an increasing of the laser threshold while decreasing the sphere-mirror

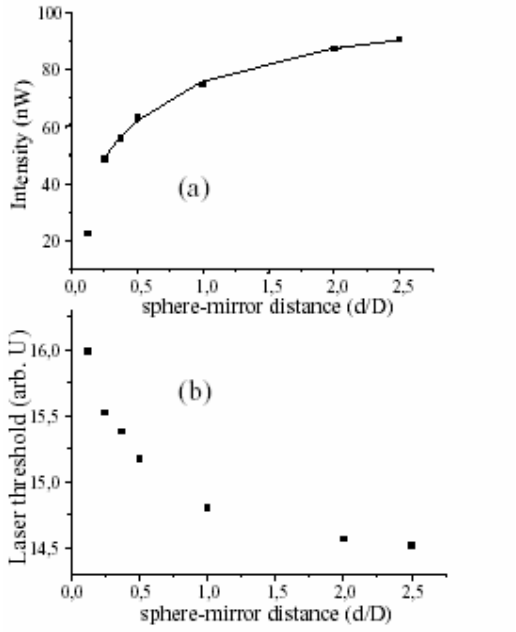

Fig. 12. Effects at 1566 *nm*(a) laser intensity *vs* sphere-mirror distance (*d=D*) (b) laser threshold *vs* sphere-mirror distance (*d=D*)

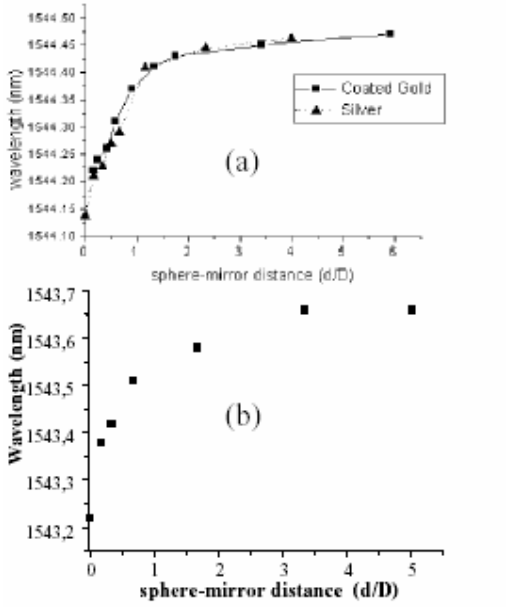

Fig. 13. (a) Blue-shift of fluorescence WGM in Er/Yb phosphate microsphere with coated gold and uncoated silver mirrors (b) Blue-shift of fluorescence WGM in Er:ZBLALiP microsphere

distance (Fig.12-b).

As the distances between sphere and mirror do not allow coupling *via* tunnel effect across the potential barrier we can assume that we observed an optical feedback due to the coupling with the external cavity constitued by the metallic mirror. In order to test this assumption we used: first, a coated gold mirror in place of the silver uncoated mirror; second, we used as active medium Er:ZBLALiP 0:08 % weight Erbium doped which allows to obtain laser action with a lower threshold (few *mW*) [31,43] than those measured with the high doping rate Er/Yb phosphate glass (few tens of *mW*). We obtained the same blue-shift behavior on all the fluorescence or laser spectra using a coated gold mirror in place of the silver uncoated mirror (Fig.13-a) or by changing the active medium (Fig.13-b) and this for different sphere diameters. Figure 13-a corresponds to results on a fluorescence WGM observed with a Er/Yb phosphate microsphere ($D \sim 60\mu m$). The zero position corresponds to our minimal distance of approach ($d = 3.5\mu m$). Figure 13-b corresponds to results on fluorescence WGM measured with a Er:ZBLALiP microsphere ($D \sim 50\mu m$) under the lasing threshold, here too, the zero position corresponds to our minimal distance of approach ($d = 3.5\mu m$).

5 Conclusion

Until recently the main disadvantage of the solid microsphere has been that the frequencies of the resonances are not tunable. For passive silica microspheres, in principle there are two methods to tune WGMs: temperature [44] and mechanical strain [45] or stretch [46].We demonstrated in this paper Red-shift effect of resonance modes in Erbium doped fluoride and phosphate microspherical lasers with increasing pump powers. With a single-frequency laser emission, we have observed a blue-shift of the emission wavelength by ~ $0.3nm$ while varying the distance sphere-mirror from $2.5D$ to $0.15D$. At the same time, depending from the lasing mode, the laser intensity was decreasing or increasing by almost 40%. In fact the distance range, the use of different mirrors and the intensity dependance lead to think to an optical feedback effect due to directional tunneling escape from nearly spherical optical resonators as reported by Lacey *et al.*[47]. Nevertheless, the combination of the two effects allows to expect the realization of tunable microspherical lasers with a constant output power.

6 Acknowledgments

The authors thank G.C. Righini, G. Nunzi Conti from CNR-IFAC Firenze - Italy, M. Mortier from LCAES-ENSCP - Paris, Z.P. Cai (Dpt of Physics), H.Y. Xu (Dpt of Electrical Engineering) from University of Xiamen - China and G.M. Stéphan (CNRS-UMR 6082) for their contributions to these works presented in this short review.

References

1. L. Collot, V. Lefèvre-Seguin, M. Brune, J.M. Raimond, S. Haroche, Europhys. Lett. 23, (1993) 327.
2. V. Lefèvre-Seguin, S. Haroche, Mater. Sci. Eng. B 48, (1997) 53.
3. R.K. Chang, A.J. Campillo, *Optical processes in microcavities* (World Scientific, Singapore, 1996).
4. B.E. Little, J.P. Laine, D.R. Lim, H.A. Haus, L.C. Kimerling, S.T. Chu, Opt. Lett. 25, (2000) 73.
5. F. Vollmer, D. Braun, A. Libchaber, M. Khoshsima, I. Teraoka, S. Arnold, Appl. Phys. Lett. 80, (2002) 4057.
6. J.L. Nadeau, V.S. Ilchenko, D. Kossakovski, G.H. Bearman, L. Maleki, Proc. of SPIE. Vol 4629, (2002) 172.
7. P.W. Barber, R.K. Chang, *Optical effects associated with small particles* (World Scientific, Singapore 1988).
8. H.B. Lin, A.J. Campillo, Phys. Rev. Lett. 73, (1994) 2440.

9. S.L. McCall, A.F.J. Levi, R.E. Slusher, S.J. Pearton, R.A. Logan, Appl. Phys. Lett. 60, (1992) 289.
10. J.M. Gérard, B. Sermage, B. Gayral, B. Legrand, E. Costard, V.T. Mieg, Phys. Rev. Lett. 81, (1998) 1110.
11. C.G.B. Garret, W. Kaiser, W.L. Long, Phys.Rev. 124, (1961) 1807.
12. T. Baer, Opt. Lett. 12, (1987) 392.
13. K. Miura, K. Tanaka, K. Hirao, J. Mat. Sci. Lett. 15, (1996) 1854.
14. V.S. Sandoghdar, F. Treussart, J. Hare, V. Lefèvre-Seguin, J.M. Raimond, S. Haroche, Phys. Rev. A 54, (1996) 1777.
15. F. Lissillour, P. Féron, N. Dubreuil, P. Dupriez, M. Poulain, G. Stéphan, Elect. Lett. 36, (2000) 1382.
16. Z.P. Cai, A. Chardon, H.Y. Xu, P. Féron, G.M. Stéphan, Opt. Comm. 203, (2002) 301.
17. S.C. Hill, R.E. Benner, C.K. Rushforth, P.R. Conwell, Appl. Opt. 23, (1984) 1680.
18. B.R. Johnson, J.O.S.A. A 11, (1994) 2055.
19. J. Stratton, *Electromagnétisme*, (Dunod, Paris 1961).
20. H.C. van de Hulst, *Light scattering by small particles*, (Wiley, New York 1981).
21. C.C. Lam, P.T. Leung, K. Young, J.O.S.A. B 9, (1992) 1585.
22. H.M. Nussenzveig, *Diffraction effects in semi-classical scattering*, (University Press, Cambridge 1992). ENSCP
23. J.P. Barton et al, J. Appl. Phys. 65 ((1989) 2900.
24. V.B. Braginsky, M.L. Gorodetsky, V.S. Ilchenko, Phys. Lett. A 137 (1989) 393.
25. J.C. Knight, G. Cheung, F. Jacques, T.A. Birks, Opt. Lett. 22 (1997) 1129.
26. M. Cai, K.J. Vahala, Opt. Lett. 26, (2001) 884.
27. F. Lissillour, D. Messager, G.M. Stéphan, P. Féron, Opt. Lett. 26, (2001) 1051.
28. N. Dubreuil, J.C. Knight, D. Leventhal, V. Sandoghdar, J. Hare, V. Lefèvre-Seguin, Opt. Lett. 20 (1995) 813.
29. V.S. Ilchenko, X.S. Yao, L. Maleki, Opt. Lett. 24 (1999) 723.
30. M.J.F. Digonnet, *Rare earth doped fiber lasers and amplifiers*, (Stanford University, USA, 1993).
31. M. Mortier, P. Goldner, P. Féron, G.M. Stéphan, H. Xu, Z. Cai, J. Non Cryst. Solids, 326 & 327, (2003) 505.
32. D.E. McCumber, Phys.Rev. 134, (1964) 299.
33. Y.D. Huang, M. Mortier, F. Auzel, Optical Materials 15, (2001) 243.
34. S. Taccheo, P. Laporta, C. Svelto, Appl.Phys.Lett. 68, (1996) 2621.
35. Z.P. Cai, H.Y. Xu, G.M. Stéphan, P. Féron, M. Mortier, Opt. Comm. 229, (2004) 311.
36. S.P. Vyatchanin, M.L. Gorodetsky, V.S. Ilchenko, Zhurnal Prikladnoi Spectroskopii 56 - 2, (1992) 274.
37. J.E. Heebner,R.W. Boyd, Q.H. Park, J.O.S.A. B 19, (2002) 722.
38. J.K.S. Poon, J. Scheuer, S. Mookherjea, G.T. Paloczi, Y. Huang, A. Yariv, Opt. Exp. 12, (2004) 90.
39. D. D. Smith, H. Chang, K. A. Fuller, J.O.S.A. B 20, (2003) 1967.
40. K.A. Fuller, Appl. Opt. 28, (1989) 3788.
41. K.A. Fuller, Appl. Opt. 30, (1991) 4716.
42. B.R. Johnson, J. Opt. Soc. Am. A 9, (1992) 1341; *errata* 10, (1993) 766.
43. G.M. Stéphan, H.Y. Xu, Z.P. Cai, P. Féron, M. Mortier, Proc. of SPIE Vol.4629, (2002) 181.
44. D.W. Vernooy, A. Furusawa, N.P. Georgiades, V.S. Ilchenko, H.J. Kimble, Phys. Rev. A 57, (1998) R2293.
45. V.S. Ilchenko, P.S. Volikov, V.L. Velichansky, F. Treussart, V. Lefèvre-Seguin, J.M. Raimond, S. Haroche, Opt. Comm. 145, (1998) 86.
46. W. von Klitzing, R. Long, V.S. Ilchenko, J. Hare, V. Lefèvre-Seguin, Opt. Lett. 26, (2001) 166.
47. S. Lacey, H. Wang, D.H. Foster, J.U. Nöckel, Phys. Rev. Lett. 91, (2004) 033902(4).